

Synthesis of three-dimensional rare-earth ions doped CNTs-GO-Fe₃O₄ hybrid structures using one-pot hydrothermal method



Guo Gao^{a,*}, Qiang Zhang^b, Xin-Bing Cheng^b, Rongjin Sun^a, Joseph G. Shapter^{c,**},
Ting Yin^a, Daxiang Cui^{a,***}

^a Institute of Nano Biomedicine and Engineering, Department of Instrument Science and Technology, Key Laboratory for Thin Film and Microfabrication Technology of Ministry of Education, School of Electronic Information and Electrical Engineering, Shanghai Jiao Tong University, Shanghai 200240, China

^b Beijing Key Laboratory of Green Chemical Reaction Engineering and Technology, Department of Chemical Engineering, Tsinghua University, Beijing 100084, China

^c School of Chemical and Physical Sciences, Flinders University, Bedford Park, Adelaide 5042, Australia

article info

Article history:

Received 10 February 2015

Received in revised form

15 June 2015

Accepted 16 June 2015

Available online 23 June 2015

Keywords:

CNTs

Fe₃O₄

Hydrothermal

LIBs

abstract

Rechargeable lithium ion batteries (LIBs) are currently the dominant power source for all sorts of electronic devices due to their low cost and high energy density. The cycling stability of LIBs is significantly compromised due to the broad satellite peak for many anode materials. Herein, we develop a facile hydrothermal process for preparing rare-earth (Er, Tm) ions doped three-dimensional (3D) transition metal oxides/carbon hybrid nanocomposites, namely CNTs-GO-Fe₃O₄, CNTs-GO-Fe₃O₄-Er and CNTs-GO-Fe₃O₄-Tm. The GO sheets and CNTs are interlinked by ultrafine Fe₃O₄ nanoparticles forming three-dimensional (3D) architectures. When evaluated as anode materials for LIBs, the CNTs-GO-Fe₃O₄ hybrid composites have a bigger broad satellite peak. As for the CNTs-GO-Fe₃O₄-Er and CNTs-GO-Fe₃O₄-Tm hybrid composites, the broad satellite peak can be completely eliminated. When the current density changes from 5 C back to 0.1 C, the capacity of CNTs-GO-Fe₃O₄-Tm hybrid composites can recover to 1023.9 mAhg⁻¹, indicating an acceptable rate capability. EIS tests show that the charge transfer resistance does not change significantly after 500 cycles, demonstrating that the cycling stability of CNTs-GO-Fe₃O₄-Tm hybrid composites are superior to CNTs-GO-Fe₃O₄ and CNTs-GO-Fe₃O₄-Er hybrid structures.

© 2015 Published by Elsevier B.V.

1. Introduction

Nowadays, the ever-rising consumption of fossil fuels has been regarded as one of the main reasons for global warming. To meet increasing energy demands of society while reducing the greenhouse gas emissions, exploring renewable and sustainable clean energy resources are urgently required. Rechargeable lithium batteries (LIBs) are deemed as one of the most promising energy storage devices for electric vehicles and energy storage system due to their environmental benignity and high energy density compared with other electrochemical energy storage systems [1,2]. The demand for high-performance LIBs has stimulated the great

efforts to develop new electrode materials to maximise high energy/power density, long cycling life, safety and low production cost [3,4]. In the numerous anode materials, transition metal oxides materials have attracted much interest because of their low cost, easy large scale fabrication and their higher theoretical capacity (e.g., 781 mAhg⁻¹ for SnO₂; 924 mAhg⁻¹ for Fe₃O₄) compared to that of conventional graphite anodes (e.g., 372 mAhg⁻¹) [5e8]. The high capacity can be attributed to the intrinsic conversion reaction process where the transition metal oxides reversibly react with lithium ions to form Li₂O (e.g., SnO₂ + 4Li⁺ + 4e⁻ → 4 Sn + 2Li₂O; Fe₃O₄ + 8Li⁺ + 8e⁻ → 3Fe + 4Li₂O). Based on the valence state of transition metal oxides, it is possible store up to 8 lithium ions per formula unit. It has been demonstrated that the capacity and cycling performance of transition metal oxides were closely related to their shapes and structures [9,10]. The main drawbacks of applying transition metal oxides as anode materials for LIBs are their poor electronic conductivity and severe volume expansion (>200%) during the repeated insertion and extraction of the lithium ions [11].

* Corresponding author.

** Corresponding author.

*** Corresponding author.

E-mail addresses: guogao@sjtu.edu.cn (G. Gao), joe.shapter@flinders.edu.au (J.G. Shapter), dx cui@sjtu.edu.cn (D. Cui).

Carbon nanotubes (CNTs) and graphene oxides (GO) sheets have high conductivity, large specific surface area and excellent mechanical properties, and they are ideal host materials for anchoring metal oxides nanocrystals [12]. Graphite is widely applied as an anode material in many commercial LIBs whereas their low theoretical capacity limit the applications for high energy density electric vehicles. Researchers have realized the development of transition metal oxides/carbon hybrid nanocomposites is of great importance to improve their electrochemical performance [13e15]. In addition, researchers found that there usually exists a capacity increasing-decreasing stage (satellite broad peak) during the cycling process for many anode nanomaterials after which the charging capacity remains relatively stable [16]. The maximum capacity value of satellite broad peak can increase up to 20% than that of the stable capacity. The reasons for satellite broad peak can be attributed to the electrolyte decomposition [17] and interfacial storage [18]. Evidently, the presence of satellite broad peak significantly influences the cycling stability of lithium storage. Luo et al. reported that the effect of rare-earth doping can reduce the crystal size, increase conductivity and enhance the diffusion rate of lithium ions and the rare-earth doping method is effective for further improving the electrochemical properties [19]. Considering the promising future application of transition metal oxides/carbon hybrid nanocomposites as anode materials of LIBs, it is important to extend the rare-earth doping strategy to improve the cycling stability of lithium storage, by reducing the intensity of satellite broad peak. However, there have been relatively few reports applying the rare-earth ion doping strategy to reduce the influence of satellite broad peak.

In this work, we developed a facile hydrothermal approach to synthesize rare-earth (Er, Tm) ions doped three-dimensional (3D) transition metal oxides/carbon hybrid nanocomposites, namely CNTs-GO-Fe₃O₄, CNTs-GO-Fe₃O₄-Er and CNTs-GO-Fe₃O₄-Tm. The oxidized CNTs and GO sheets are assembled into 3D architectures by the interlinkage of ultrafine Fe₃O₄ nanocrystals in the hydrothermal system (Scheme 1). When evaluated as anode materials for LIBs, the CNTs-GO-Fe₃O₄ hybrid composites have a bigger satellite broad peak varying from the 33rd cycle to the 801th cycle under a high current density of 5 C. As for the CNTs-GO-Fe₃O₄-Er and CNTs-GO-Fe₃O₄-Tm hybrid composites, the capacity stabilized at 218.4 mAhg⁻¹ on the 200th cycle, and the satellite broad peak can be completely eliminated. Even with a significant increase of current density from 1 C to 5 C, the rare-earth doping hybrid composites (CNTs-GO-Fe₃O₄-Er and CNTs-GO-Fe₃O₄-Tm) could still maintain a stable capacity after 200 cycles. When the current density changes back to 0.1 C, the capacity of CNTs-GO-Fe₃O₄-Tm composites can recover to 1023.9 mAhg⁻¹, indicating an acceptable rate capability. EIS tests showed that the capacitive arc diameter of the Tm doped hybrid structures did not change significantly after 500 cycles, suggesting that the cycling stability of this hybrid

composite is superior the other hybrid structures prepared.

2. Experimental section

2.1. Synthesis of three-dimensional CNTs-GO-Fe₃O₄, CNTs-GO-Fe₃O₄-Er and CNTs-GO-Fe₃O₄-Tm hybrid structures

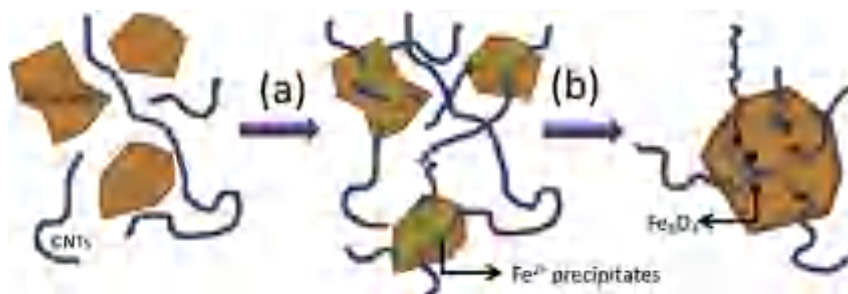
The multi-wall CNTs were prepared following our reported nano-agglomerate fluidized bed reactor method [20], and the GO sheets were prepared by the modified Hummers method [21]. After the synthesis of CNTs, CNTs were then oxidized by a mixed acid solution of HNO₃ and H₂SO₄ in the volume ratio of 1:3 at 80 °C for 20 min. The oxidized CNTs were centrifuged by a high-speed centrifuge, washed by deionized water and dried in a freeze-drying apparatus for 24 h. Typically, 15 mL of oxidized CNTs solution (0.01 g mL⁻¹) was mixed with 10 mL GO sheets solution (0.001 g mL⁻¹), then 10 mL ferric citrate (0.1 M) was added into the mixture. After that, 1 g FeSO₄·7H₂O and 0.1 g vitamin C (Vc) were added. After stirring the mixture for 10 min, 5 mL NaOH solution (0.4 M) was gradually added. The mixture was vigorously stirred for 30 min. As for the Er³⁺ and Tm³⁺ doping process, an additional 5 mL ErCl₃ (0.2 M) and 5 mL TmCl₃ (0.2 M) was added into the mixture, respectively. The obtained mixture in the absence and presence of rare-earth ions (Er³⁺, Tm³⁺) was then transferred into a Teflon-lined stainless autoclave and heated to 180 °C for 20 h. After reaction, the products were filtered, washed with deionized water and dried in a freeze-drying apparatus for 24 h.

2.2. Characterization

All of the samples were characterized by an X-ray powder diffractometer (XRD, Rigaku, Japan), scanning electron microscopy (SEM, FEI-Sirion 200), transmission electron microscopy (TEM, JEM-2010), high-resolution transmission microscopy (HRTEM, JEM-2010) and selected area electron diffraction (SAED, JEM-2010). The thermal analysis was determined by a thermogravimetric analyzer (Pyris 1 TGA, PerkinElmer, USA) at a heating rate of 10 °C min⁻¹ from 20 °C to 900 °C. Raman measurements were performed at room temperature using a SENTERRA R200 Raman microscope.

2.3. Electrochemical measurements

The electrochemical properties of CNTs-GO-Fe₃O₄, CNTs-GO-Fe₃O₄-Er and CNTs-GO-Fe₃O₄-Tm hybrid structures as the anode materials of lithium ion batteries were measured using CR2025 coin cells. Working electrodes were fabricated by mixing 80 wt % active materials with 10 wt % acetylene black and 10 wt % polyvinylidene fluoride (PVDF) in the N-methyl-2-pyrrolidone (NMP) solvent, which was then coated on a copper foil. After solvent evaporation, the electrodes were dried in a vacuum oven at 120 °C



Scheme 1. Formation process of three-dimensional (3D) Fe₃O₄/carbon hybrid nanocomposites in the hydrothermal system. The CNTs and GO sheets are interlinked together by the Fe²⁺ precipitates (a) and after hydrothermal reaction at 180 °C for 20 h, the Fe²⁺ precipitates decompose into Fe₃O₄ (b).

for 12 h. Then the electrodes were cut into circular sheets, and then pressed under a pressure of 2 MPa. Coin cells were assembled in an argon-filled glovebox in the presence of oxygen scavenger and sodium drying agent. The hybrid composites act as working electrode, metallic lithium as counter/reference electrode. 1 M LiPF₆ in ethylene carbonate, diethyl carbonate and ethylmethyl carbonate (EC/DMC/EMC, volume ratio of 1:1:1) was used as electrolyte and Celgard 2400 polypropylene as separator.

3. Results and discussion

Fig. 1a shows the powder XRD patterns of the synthesized CNTs-GO-Fe₃O₄, CNTs-GO-Fe₃O₄-Er and CNTs-GO-Fe₃O₄-Tm hybrid structures. Two diffraction peaks at $2\theta = 26.1^\circ$ and 42.7° can be attributed to the (002) and (110) planes of CNTs, respectively. Other small diffraction peaks can be attributed to the inverse cubic spinel Fe₃O₄ structure (JCPDS No.19-629). No GO peaks were detected which was possibly attributed to the fact that the amount of GO in the samples is quite low. As for the XRD patterns of CNTs-GO-Fe₃O₄, the diffraction peaks of Fe₃O₄ were very weak, indicating that the amount of Fe₃O₄ in CNTs-GO-Fe₃O₄ hybrid composites was low or the Fe₃O₄ has an amorphous structure. After doping Er³⁺ ions, the diffraction peaks of CNTs become stronger. Some small diffraction peaks arising from Fe₃O₄ structures were also observed. As for the Tm³⁺ ions doping composites, the peaks of CNTs become even stronger but the peaks of Fe₃O₄ disappear. From the XRD analysis, we can see that the structural integrity of the oxidized CNTs in the CNTs-GO-Fe₃O₄ hybrid composites was improved after the rare-earth ions doping process. It is known that the oxidation of CNTs by mixed acid will lead to the decrease of structural integrity. Evidently, rare-earth ions doping process is helpful for the improvement of structural integrity. Fig. 1b shows the Raman spectra of the CNTs-GO-Fe₃O₄, CNTs-GO-Fe₃O₄-Er and CNTs-GO-Fe₃O₄-Tm hybrid structures. It is obvious that the Raman spectra exhibit two characteristic bands: the tangential (vibrations along

the tube axis) stretching G mode (1578.5 cm^{-1}) and the D mode (1343.3 cm^{-1}). It is evident that the two scattering peaks become stronger after the rare-earth ion doping. Usually, the intensity ratio of 'D' peak (I_D) to 'G' peak (I_G) was used to evaluate the amount of defects in CNTs [22]. The Raman spectra of the composites shows that a low intensity ratio of the D band to the G band ($I_D/I_G = 0.928$ for CNTs-GO-Fe₃O₄, $I_D/I_G = 0.875$ for CNTs-GO-Fe₃O₄-Er and $I_D/I_G = 0.786$ for CNTs-GO-Fe₃O₄-Tm), indicating that the defect density of oxidized CNTs in the CNTs-GO-Fe₃O₄ hybrid composites has been improved. Moreover, the peak width of rare-earth ions doped hybrid composites is larger than that of the CNTs-GO-Fe₃O₄ samples. Fig. 1c shows the TGA curves in air for the CNTs-GO-Fe₃O₄, CNTs-GO-Fe₃O₄-Er and CNTs-GO-Fe₃O₄-Tm hybrid structures. The initial 5.5% weight loss (up to 102°C) is due to the evaporation of physical adsorbed water on the samples. As for CNTs-GO-Fe₃O₄, CNTs-GO-Fe₃O₄-Er and CNTs-GO-Fe₃O₄-Tm hybrid structures, the final mass loss temperature is about 500 , 567.6 and 604.7°C , respectively. Evidently, the rare-earth ions doping process has improved the thermal stability of the oxidized CNTs in the CNTs-GO-Fe₃O₄ hybrid composites. According to the TGA curves, the carbon contents of CNTs-GO-Fe₃O₄ hybrid composites are about 70.2, 88.1 and 81.2% by weight.

The morphology of the CNTs-GO-Fe₃O₄ hybrid structures was shown in Fig. 2. From Fig. 2aeb, it is clearly seen that numerous CNTs are well attached on the surface of GO sheets indicating formation of 3D architectures. The width of GO sheets can reach several micrometers. The higher magnification TEM image of Fig. 2c clearly shows that the GO sheets and CNTs are interlinked together by the ultrafine Fe₃O₄ nanoparticles. The HRTEM image of Fig. 2d shows the diameter of Fe₃O₄ nanoparticles is about $5\text{--}10\text{ nm}$. Parallel crystal lattice fringes of Fe₃O₄ nanoparticles are discerned, suggesting that the majority of Fe₃O₄ nanoparticles have a single crystal feature. The fringe lattice was measured to be 0.483 nm , which is close to that of the (111) lattice spacing in the Fe₃O₄ (0.485 nm). This confirmed that the small particles in the hybrid

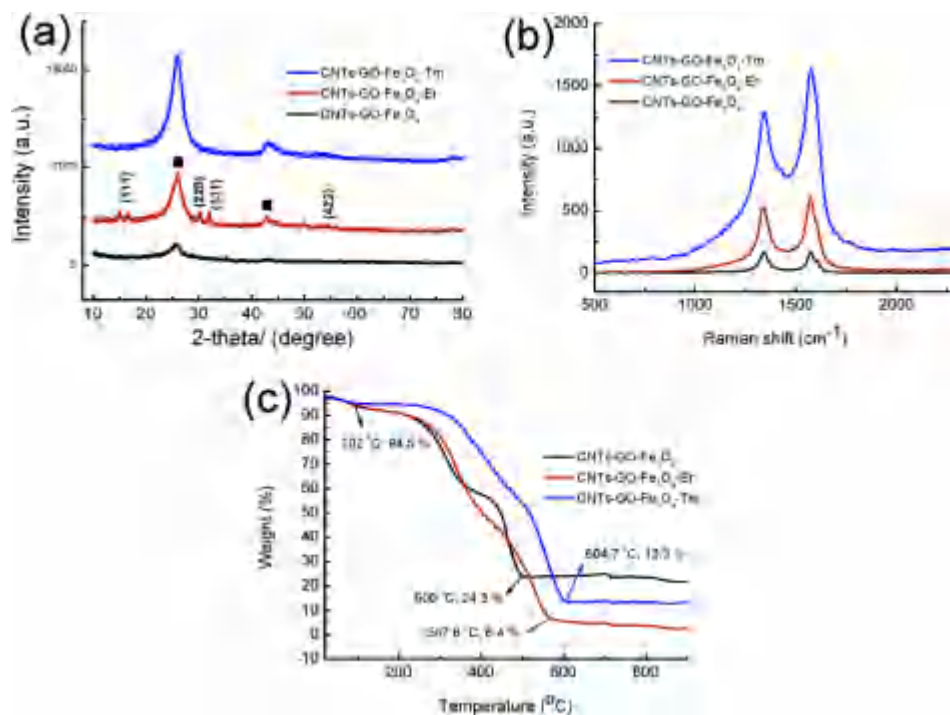


Fig. 1. XRD patterns (a), the diffraction peaks of CNTs were indexed by a black square, Raman spectra (b) and TGA curves of the CNTs-GO-Fe₃O₄, CNTs-GO-Fe₃O₄-Er and CNTs-GO-Fe₃O₄-Tm hybrid structures (c).

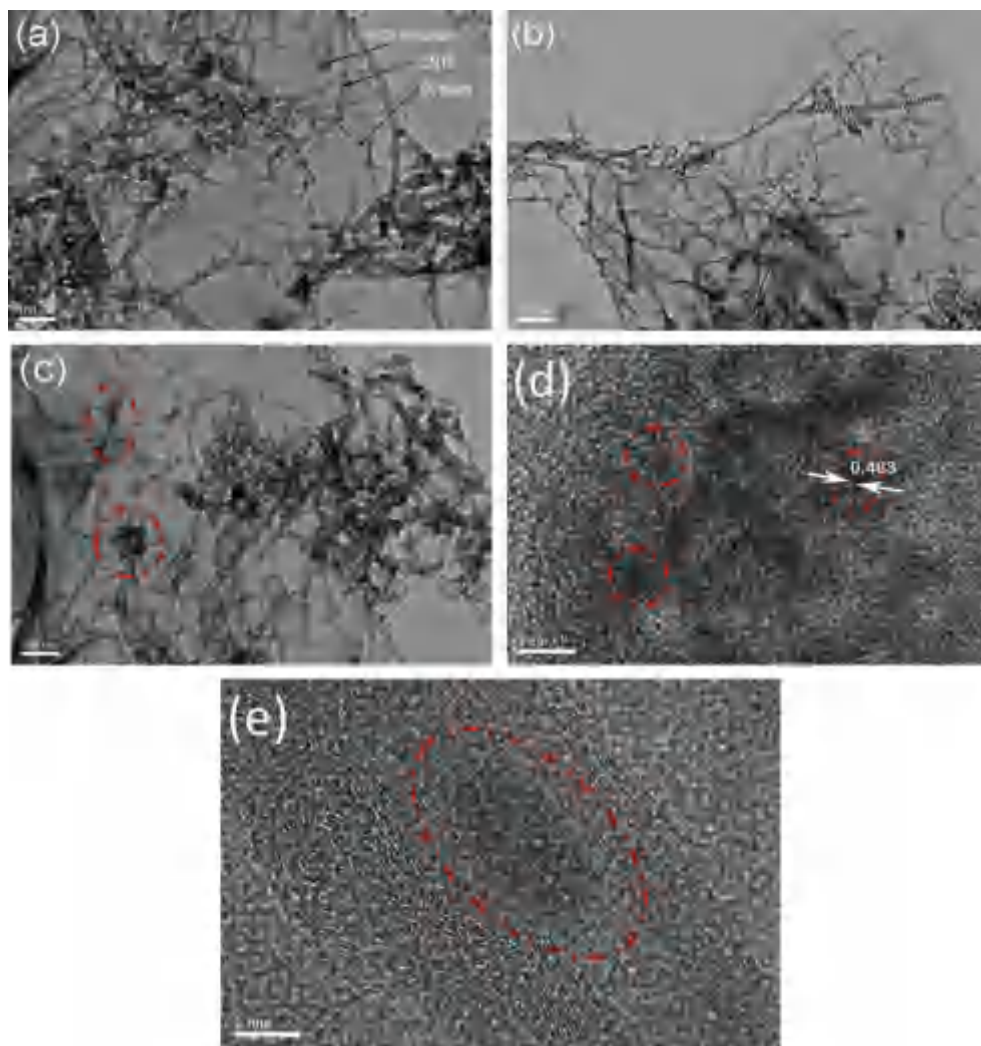


Fig. 2. TEM and HRTEM images of the synthesized CNTs-GO-Fe₃O₄ hybrid structures in the hydrothermal system (aee).

composites are the Fe₃O₄ components. Fig. 2e shows that a few Fe₃O₄ nanoparticles were embedded into the CNTs. The lower loading amount of Fe₃O₄ into CNTs can be attributed to the fact that the oxidized CNTs were initially dispersed in deionized water, not directly dispersed in the ferric citrate solution. It is also clear that the oxidized CNTs have a relatively high defect density. The surface of oxidized CNTs and GO sheets has many different types of oxygen functionalities (e.g., -COOH, -OH and -C=O), which could act as the active sites for the deposition of Fe²⁺ precipitates. In the presence of Fe²⁺ ions, the oxidized CNTs and GO sheets will be interlinked together by the complex of Fe²⁺ ions through the rich oxygen functionalities. When the NaOH solution was added, the Fe²⁺ precipitates formed. During the hydrothermal reaction, the thermal-decomposition of Fe²⁺ precipitates will lead to the formation of Fe₃O₄ nanoparticles which will act as the robust welding point between the oxidized CNTs and GO sheets. Finally, the 3D CNTs-GO-Fe₃O₄ hybrid structures are formed.

After the CNTs-GO-Fe₃O₄ hybrid structures were doped with Er³⁺ and Tm³⁺ ions, the morphology of products do not change significantly. Fig. 3a and c show a TEM image of the synthesized CNTs-GO-Fe₃O₄-Er and CNTs-GO-Fe₃O₄-Er-Tm hybrid structures, respectively. The CNTs are well attached on the surface of GO sheets. The HRTEM images of Fig. 3b and d show that the oxidized CNTs have a high defect density for the CNTs-GO-Fe₃O₄-Er and

CNTs-GO-Fe₃O₄-Tm hybrid structures. The crystallinity improvement of the oxidized CNTs implied that the defects of CNTs during the oxidation process by mixed acid have been reduced.

Because of the high theoretical Li-storage capacity (924 mAhg⁻¹ for Fe₃O₄), the synthesized 3D CNTs-GO-Fe₃O₄, CNTs-GO-Fe₃O₄-Er and CNTs-GO-Fe₃O₄-Tm hybrid structures were tested as anode materials for lithium ion batteries under high current densities (1 C and 5 C). Fig. 4a shows the cycling performance of the 3D CNTs-GO-Fe₃O₄, CNTs-GO-Fe₃O₄-Er and CNTs-GO-Fe₃O₄-Tm hybrid structures under a current density of 1 C for 680 long-term cycles. As for the CNTs-GO-Fe₃O₄ hybrid structures electrode, the capacity rapidly decreased during the first 16 cycles. The initial discharge capacity is 872.5 mAhg⁻¹, and the capacity of 16th cycle is 431.3 mAhg⁻¹. The decrease of capacity was attributed to the formation of an inorganic solid electrolyte interface (SEI) film. After the 16 cycles, the capacity starts to increase arriving at a maximum capacity value (737.5 mAhg⁻¹) at the 116th cycle. This process is attributed to the electrolyte decomposition and the reaction of lithium ions with oxygen-containing groups in the CNTs layer [23]. After the 116 cycles, the capacity rapidly decreased and stabilized at about 332.1 mAhg⁻¹ at the 358th cycle. The satellite broad peak was evident from the 14th cycle to the 400th cycle, and then the cycling behaviour stabilized for later cycles. Evidently, the presence of satellite broad peak has significantly influenced the cycling

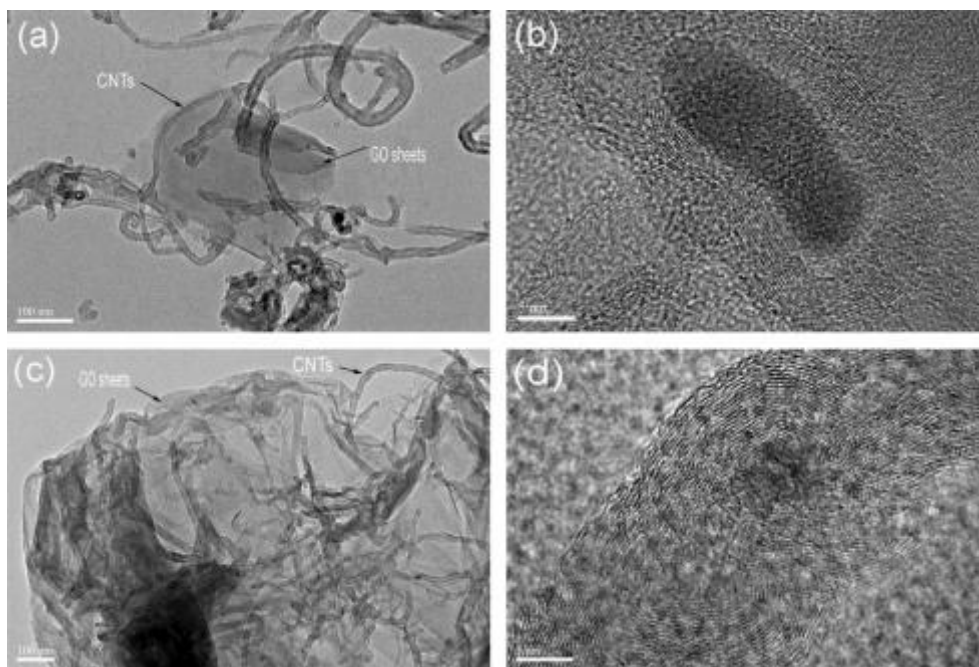


Fig. 3. TEM and HRTEM images of the synthesized CNTs-GO-Fe₃O₄-Er (a, b) and CNTs-GO-Fe₃O₄-Tm (c, d) hybrid structures in the hydrothermal system.

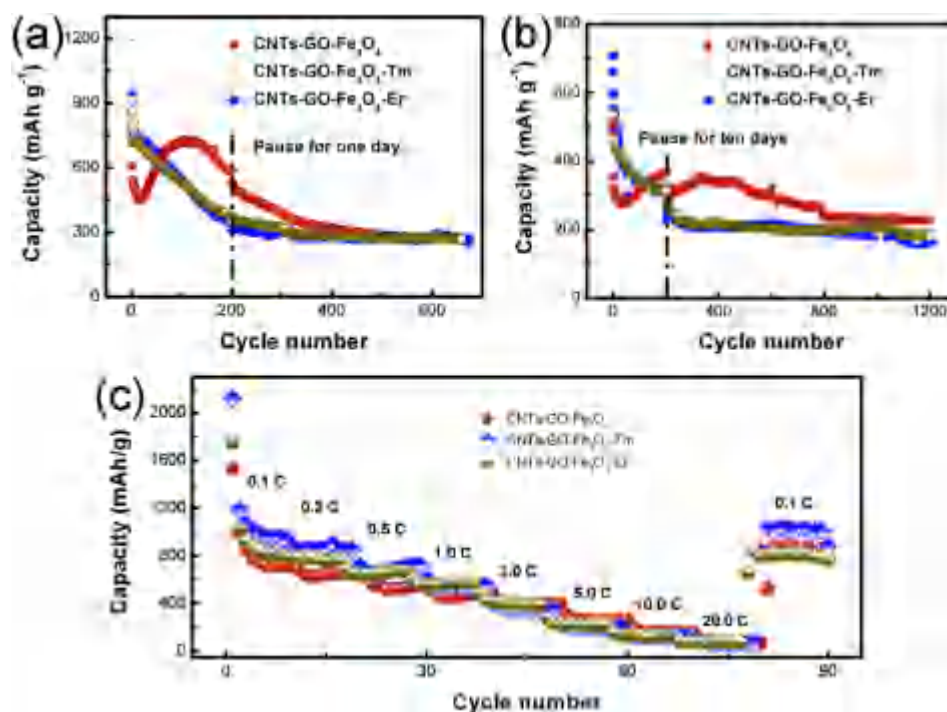


Fig. 4. Cycling performance of the synthesized CNTs-GO-Fe₃O₄, CNTs-GO-Fe₃O₄-Er and CNTs-GO-Fe₃O₄-Tm hybrid structures at the current density of 1 C (a), 5 C (b) and rate performance of hybrid composites electrodes at different current density (c).

stability of LIBs. As for the CNTs-GO-Fe₃O₄-Er and CNTs-GO-Fe₃O₄-Tm hybrid structures, it is evident that the satellite broad peak was completely eliminated. Under the current density of 1 C, the cycling performance curves of CNTs-GO-Fe₃O₄-Er and CNTs-GO-Fe₃O₄-Tm hybrid structures presented the similar shapes. From the 6th cycle to the 200th cycle, the capacity gradually decreased linearly and stabilized at 341.9 mAhg⁻¹. Clearly, the cycling stability of electrodes have been significantly improved due the rare-earth doping

process. Fig. 4b shows the cycling performance of the 3D CNTs-GO-Fe₃O₄, CNTs-GO-Fe₃O₄-Er and CNTs-GO-Fe₃O₄-Tm hybrid structures under a high current density of 5 C for 1215 longer-term cycles. As for CNTs-GO-Fe₃O₄ hybrid composites, there is a bigger satellite broad peak appearing from the 33rd cycle to the 801th cycle. The increase of current density enlarges the width interval of satellite broad peak. The capacity rapidly fades during the initial cycles to a minimum of 268.7 mAhg⁻¹ at the 33rd cycle. Then, the

capacity increases, and forming the satellite broad peak. It can be seen that the capacity stabilized at 245.1 mAhg^{-1} after the 801th cycle. As for the CNTs-GO-Fe₃O₄-Er and CNTs-GO-Fe₃O₄-Tm hybrid structures, the capacity stabilized at 218.4 mAhg^{-1} on the 200th cycle. Although the significant increase of current density from 1 C to 5 C, the rare-earth doping hybrid composites (CNTs-GO-Fe₃O₄-Er and CNTs-GO-Fe₃O₄-Tm) still maintain the capacity at a stable value after 200 cycles. Clearly, the rare-earth ions doping process has improved the cycling stability of the CNTs-GO-Fe₃O₄ hybrid electrodes. The rate performance of the 3D CNTs-GO-Fe₃O₄, CNTs-GO-Fe₃O₄-Er and CNTs-GO-Fe₃O₄-Tm hybrid structures was tested at various current densities, as shown in Fig. 4c. As for CNTs-GO-Fe₃O₄ composites, the discharge capacities of electrodes are 707.7, 638.8, 542.6, 452.5, 419.6, 287.5, 193.4 and 70.3 mAhg^{-1} at current densities of 0.1, 0.2, 0.5, 1.0, 2.0, 5.0, 10.0 and 20.0 C, respectively. As for CNTs-GO-Fe₃O₄-Er composites, the discharge capacities of electrodes are 852.9, 783.3, 665.1, 580.5, 405.8, 231.2, 136.3 and 84.7 mAhg^{-1} at current densities of 0.1, 0.2, 0.5, 1.0, 2.0, 5.0, 10.0 and 20.0 C, respectively. As for CNTs-GO-Fe₃O₄-Tm composites, the discharge capacities of electrodes are 986.1, 891.9, 745.5, 599.1, 401.1, 244.9, 155.6 and 103.3 mAhg^{-1} at current densities of 0.1, 0.2, 0.5, 1.0, 2.0, 5.0, 10.0 and 20.0 C, respectively. It is noticed that the capacity of CNTs-GO-Fe₃O₄-Tm composites can recover to 1023.9 mAhg^{-1} when the current density changes back to 0.1 C, which indicated an acceptable rate capability.

Cyclic voltammetry (CV) measurements of the synthesized CNTs-GO-Fe₃O₄, CNTs-GO-Fe₃O₄-Er and CNTs-GO-Fe₃O₄-Tm hybrid structures were carried out in the voltage range 0e3.0 V at a scan rate of 0.5 mVs^{-1} , as shown in Fig. 5. Fig. 5a shows the CV curves of CNTs-GO-Fe₃O₄ hybrid composites. In the first cycle, the slight cathodic peak at around 0.8 V was observed due to the reduction of both Fe³⁺ and Fe²⁺ to Fe⁰ and the irreversible reaction relating to the electrolyte decomposition [24]. At this stage, the irreversible capacity loss was attributed to the conversion of Fe₃O₄ to Fe and the

formation of Li₂O (Fe₃O₄ + 8e⁻ + 8Li⁺ / 3Fe⁰ + 4Li₂O, xLi⁺ + Fe⁰ + xe⁻ / Li_xFe). A broad anodic peak at around 1.4 V was related to the reversible oxidation reaction of Fe⁰ to Fe²⁺ and Fe⁰ to Fe³⁺ [25]. For the subsequent four cycles, both the peak current and the integrated area of the anodic peaks nearly overlap, indicating a low capacity loss of lithium insertion and extraction after the first cycle. Fig. 5b and c show the CV curves of CNTs-GO-Fe₃O₄-Er and CNTs-GO-Fe₃O₄-Tm hybrid structures, respectively. Clearly, the CV curves are similar with that of CNTs-GO-Fe₃O₄ hybrid composites, indicating the rare-earth doping process does not significantly influence the anodic and cathodic reaction processes.

As for the CV curves of CNTs-GO-Fe₃O₄, CNTs-GO-Fe₃O₄-Er and CNTs-GO-Fe₃O₄-Tm hybrid structures, the cathodic and anodic peaks close to 0 V and 0.15 V after the first cycle, which was attributed to the lithium ion insertion and extraction from CNTs [26]. In order to obtain further understanding for the synthesized CNTs-GO-Fe₃O₄, CNTs-GO-Fe₃O₄-Er and CNTs-GO-Fe₃O₄-Tm hybrid structures, electrochemical impedance spectroscopy (EIS) was employed to investigate the reaction kinetics of different electrodes, as shown in Fig. 5d. The EIS spectra of CNTs-GO-Fe₃O₄, CNTs-GO-Fe₃O₄-Er and CNTs-GO-Fe₃O₄-Tm hybrid composites are all composed of a depressed quasi-semicircle and a straight sloping line. The capacitive arc was related to the reaction resistance, and the straight line was assigned to the diffusion of lithium ions into electrode materials or so-called Warburg diffusion [27]. As for the three electrodes before and after cycling, only the capacitive arc diameter of CNTs-GO-Fe₃O₄-Tm hybrid structures did not change significantly, indicating that the Tm³⁺ ions doping hybrid composites could maintain the cycling stability of electrodes. It is clear that the presence of the rare earth ions eliminates the broad satellite in the cycling profile. The formation of 'satellite broad peak' is attributed to the electrolyte decomposition and the reaction of lithium ions with oxygen-containing groups in the oxidized CNTs components [23]. It is known that the rare-earth ions have good

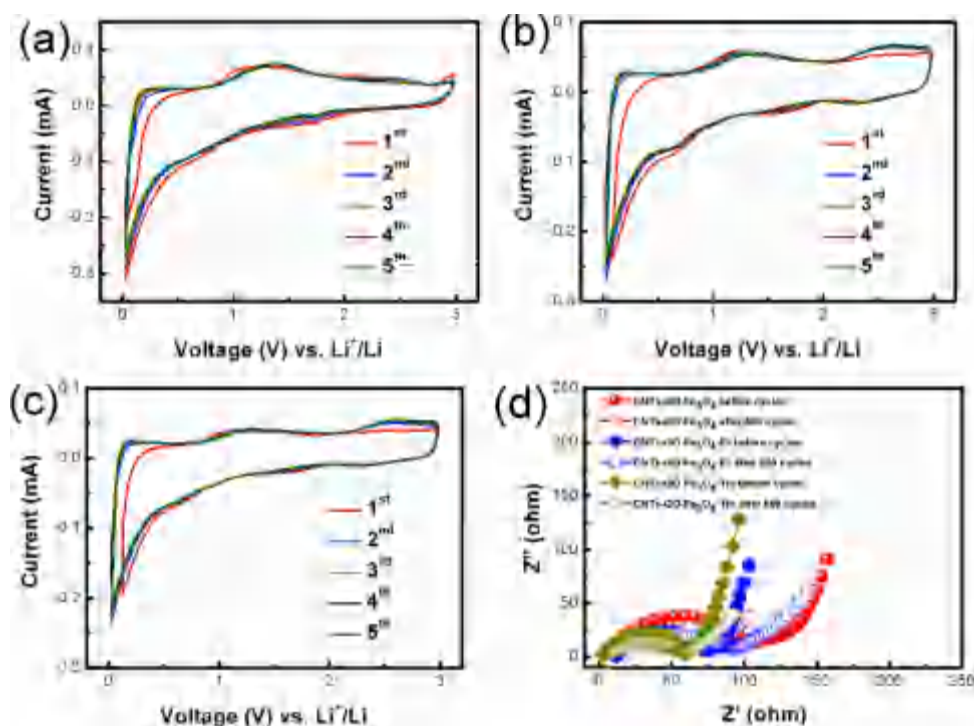


Fig. 5. Cyclic voltammograms of the synthesized CNTs-GO-Fe₃O₄ (a), CNTs-GO-Fe₃O₄-Er (b) and CNTs-GO-Fe₃O₄-Tm (c) hybrid structures at a scan rate of 0.5 mVs^{-1} , Nyquist plots of the hybrid composites electrodes before and after 500 cycles (d).

complexing ability to oxygen-containing groups. During the synthesis of CNTs-GO-Fe₃O₄ hybrid composites in hydrothermal system, the addition of rare-earth ions will significantly reduce the active sites of oxygen-containing groups. Therefore, the rare-earth ions doped CNTs-GO-Fe₃O₄ hybrid composites could suppress the 'satellite broad peak'. Additionally, the presence of rare-earth ions will also improve the structural integrity of the oxidized CNTs in the CNTs-GO-Fe₃O₄ hybrid composites, which has been demonstrated by our XRD and Raman results. It has been demonstrated that the rare-earth doping can reduce the crystal size, increase conductivity and enhance the diffusion rate of lithium ions, and thereafter further improving the electrochemical performance of LIBs [19]. The initial discharge capacity is 872.5 mAhg⁻¹, and the capacity of 16th cycle is 431.3 mAhg⁻¹. The decrease of capacity was attributed to the formation of inorganic solid electrolyte interface (SEI) film. After the 16 cycles, the capacity has an increasing trend, and arriving at a maximum capacity value (737.5 mAhg⁻¹) at the 116th cycle. This process is attributed to the electrolyte decomposition and the reaction of lithium ions with oxygen-containing groups in the CNTs layer [23]. After the 116 cycles, the capacity rapidly decreased and stabilized at about 332.1 mAhg⁻¹ at the 358th cycle. The satellite broad peak varied from the 14th cycle to the 400th cycle, and stabilized after the following cycling. Evidently, the presence of satellite broad peak has significantly influenced the cycling stability of LIBs. Compared with the hybrid materials in the literature [18], the performance of our synthesized rare-earth doped CNTs-GO-Fe₃O₄ hybrid materials is still comparable with the state-of-the-art of Fe₃O₄-based electrodes with good cycling and rate performance. The reported capacity of satellite broad peak could increase up to 20% compared to that of the stable capacity, which will significantly influence the cycling stability and safety of lithium ion battery. As for our synthesized rare-earth doped CNTs-GO-Fe₃O₄ hybrid composites, the capacity can stabilize at 218.4 mAhg⁻¹ at the 200th cycle, much earlier than other systems, and the satellite broad peak can be completely eliminated. Even at high current density (5 C), the rare-earth doped hybrid composites still maintain a stable capacity after 200 cycles. Furthermore, when the current density returned to 0.1 C, the composites can recover to 1023.9 mAhg⁻¹ which revealing an acceptable electrochemical performance. From the electrochemical tests, we can safely conclude that the rare-earth ions doping process can improve the cycling stability of transition metal oxides/carbon hybrid electrodes. Moreover, the electrochemical performance of Tm³⁺ ion doped composites are superior to that of Er³⁺ ion doped composites.

4. Conclusions

In summary, a facile hydrothermal method for preparing rare-earth ions doped CNTs-GO-Fe₃O₄, CNTs-GO-Fe₃O₄-Er and CNTs-

GO-Fe₃O₄-Tm composites have been demonstrated. When evaluated as anode materials for LIBs, the CNTs-GO-Fe₃O₄ hybrid composites have a bigger satellite broad peak whereas the rare-earth doped CNTs-GO-Fe₃O₄-Er and CNTs-GO-Fe₃O₄-Tm hybrid composites completely eliminated the satellite broad peak. The electrochemical tests showed that CNTs-GO-Fe₃O₄-Tm hybrid composites are superior to CNTs-GO-Fe₃O₄ and CNTs-GO-Fe₃O₄-Er hybrid composites because its recycling ability is the most stable likely due to its stable microstructure. The EIS tests showed that the charge transfer resistance did not change significantly after 500 cycles, demonstrating that the cycling stability of CNTs-GO-Fe₃O₄-Tm hybrid composite.

Acknowledgment

We thank the financial support by Chinese 973 Project (2010CB933901, 2015CB931802), National Natural Science Foundation of China (81225010, 21306102, 81327002), and 863 High-Tech project of China (2014AA020701, 2012AA0022603).

References

- [1] Y. Wang, H. Li, P. He, E. Hosono, H. Zhou, *Nanoscale* 2 (2010) 1294.
- [2] Z. Wang, L. Zhou, X.W. Lou, *Adv. Mater.* 24 (2012) 1903.
- [3] Q. Zhang, E. Uchaker, S.L. Candelaria, G. Cao, *Chem. Soc. Rev.* 42 (2013) 3127.
- [4] X. Chen, C. Li, M. Grätzel, R. Kosteckii, S.S. Mao, *Chem. Soc. Rev.* 41 (2012) 7909.
- [5] C. Zhang, J. Chen, Y. Zeng, X. Rui, J. Zhu, W. Zhang, C. Xu, T.M. Lim, H.H. Hng, *Q. Yan, Nanoscale* 4 (2012) 3718.
- [6] J. Liu, Y. Li, X. Huang, R. Ding, Y. Hu, J. Jiang, L. Liao, *J. Mater. Chem.* 19 (2009) 1859.
- [7] P. Wu, N. Du, H. Zhang, J. Yu, Y. Qi, D. Yang, *Nanoscale* 3 (2011) 746.
- [8] Z. Xiao, Y. Xia, Z. Ren, Z. Liu, G. Xu, C. Chao, X. Li, G. Shen, G. Han, *J. Mater. Chem.* 22 (2012) 20566.
- [9] N. Li, G. Liu, C. Zhen, F. Li, L.L. Zhang, H.M. Cheng, *Adv. Funct. Mater.* 21 (2011) 1717.
- [10] Z.Y. Wang, D.Y. Luan, S. Madhavi, Y. Hu, X.W. Lou, *Energy Environ. Sci.* 5 (2012) 5252.
- [11] R. Wang, C. Xu, J. Sun, L. Gao, C. Lin, *J. Mater. Chem. A* 1 (2013) 1794.
- [12] H.L. Wang, Y. Yang, Y.Y. Liang, L.F. Cui, H.S. Casalongue, Y.G. Li, G.S. Hong, Y. Cui, H.J. Dai, *Angew. Chem. Int. Ed.* 50 (2011) 7364.
- [13] H. Wang, H. Dai, *Chem. Soc. Rev.* 42 (2013) 3088.
- [14] X. Zhou, Z. Dai, S. Liu, J. Bao, Y.G. Guo, *Adv. Mater.* 26 (2014) 3943.
- [15] L. Zhang, G. Zhang, H.B. Wu, L. Yu, X.W. Lou, *Adv. Mater.* 25 (2013) 2589.
- [16] L. Li, K.H. Seng, Z. Chen, Z. Guo, H.K. Liu, *Nanoscale* 5 (2013) 1922.
- [17] S. Grugeon, S. Laruelle, L. Dupont, J.M. Tarascon, *Solid State Sci.* 5 (2003) 859.
- [18] P. Balaya, H. Li, L. Kienle, J. Maier, *Adv. Funct. Mater.* 13 (2003) 621.
- [19] S. Luo, Y. Tian, H. Li, K. Shi, Z. Tang, Z. Zhang, *J. Rare Earth* 28 (2010) 439.
- [20] F. Wei, Q. Zhang, W.Z. Qian, H. Yu, Y. Wang, G.H. Luo, G.H. Xu, D.Z. Wang, *Powder Technol.* 183 (2008) 10.
- [21] W.S. Hummers, R.E. Offeman, *J. Am. Chem. Soc.* 80 (1958) 1339.
- [22] T. Muraliganth, A.V. Murugan, A. Manthiram, *Chem. Commun.* (2009) 7360.
- [23] S.M. Yuan, J.X. Li, L.T. Yang, L.W. Su, L. Liu, Z. Zhou, *ACS Appl. Mater. Interf.* 3 (2011) 705.
- [24] Y. Chen, H. Xia, L. Lu, J. Xue, *J. Mater. Chem.* 22 (2012) 5006.
- [25] Y.Z. Piao, H.S. Kim, Y.E. Sung, T. Hyeon, *Chem. Commun.* 46 (2010) 118.
- [26] G. Che, B.B. Lakshmi, E.R. Fisher, C.R. Martin, *Nature* 393 (1998) 346.
- [27] X. Jia, Z. Chen, A. Suwarnasarn, L. Rice, X. Wang, H. Sohn, Q. Zhang, B. Wu, F. Wei, Y. Lu, *Energy Environ. Sci.* 5 (2012) 6845.